Photon-photon correlations from a pair of strongly coupled two-level emitters

Elnaz Darsheshdar,[1,*] Mathilde Hugbart,[2,†] Romain Bachelard,[1,‡] and Celso Jorge Villas-Boas[1,§]
[1]*Departamento de Física, Universidade Federal de São Carlos, P.O. Box 676, 13565-905 São Carlos, São Paulo, Brazil*
[2]*Université Côte d'Azur, CNRS, INPHYNI, France*

(Received 25 November 2020; revised 15 April 2021; accepted 19 April 2021; published 6 May 2021)

We investigate two-color photon correlations in the light emitted by two strongly driven, strongly interacting two-level emitters. The correlations are interpreted introducing the collective dressed states picture, which allows us to describe both bunching and antibunching based on the allowed and prohibited transitions. At odds from weakly interacting emitters, the strong interaction lifts the degeneracy of the energy differences between the different states, leading to a temporal breaking of symmetry for the correlations: photons of different frequencies may not be emitted in any order. Finally, we show that most of the virtual processes, which involve pairs of photons, yield nonclassical correlations when the sum of their energies fits any of the interaction-induced sidebands in the emitted spectrum. In particular, depending on the frequency of the emitted photons, correlations strong enough to violate Bell inequalities can appear.

DOI: 10.1103/PhysRevA.103.053702

I. INTRODUCTION

Two-level emitters essentially behave as classical oscillators when they are weakly driven, and the light elastically scattered by such systems presents a range of optical phenomena that can be understood using the tools of linear optics: dispersion, Rayleigh scattering, and even cooperative phenomena such as superradiance [1]. Yet, when strongly driving a single emitter, inelastic components appear in the scattering, a signature of the nonlinear reaction of the atom to the field. A "Mollow triplet" emerges in the fluorescence spectrum, composed of a carrier centered at the laser frequency, and two symmetric sidebands shifted away by the Rabi frequency of the driving field [2]. Of particular interest are the correlations between the photons emitted from the two sidebands, which were originally measured in atomic systems [3] and extensively studied theoretically [4–6]. Recently, the field has drawn renewed attention in the context of quantum dots, with the recent measurement of photon (anti)correlations between sidebands [7], thus demonstrating the potential of artificial atoms as sources of heralded photons.

In this context, the coupling of emitters gives access to new control parameters, as interaction-induced resonances and interferences phenomena arise [8], which could be used to tune the correlations in the emitted photons. Indeed, the coupling of the emitters through common radiation modes results in dipole-dipole interactions, which manifest in both the exchange of excitations and cooperative decay processes [9,10]. As a consequence, the fluorescence spectrum of strongly driven atoms presents sidebands [11–13] which, for a weak interaction, appear at twice the Rabi frequency from the carrier. Such effects are expected to show up, for instance, in many-atom dilute clouds, with the resonant optical thickness playing the role of a cooperativity parameter [14].

Nevertheless, the diversity of photon-photon correlations emitted from strongly interacting systems has barely been explored, despite its wide range of applications. For instance, photon-photon correlation is a key ingredient for a plethora of applications in quantum information science, such as secure quantum communication [15] and quantum metrology [16], and also to test fundamental aspects of the quantum theory itself [17]. From a technical point of view, the recent development of the so-called sensor method [18], where photons emitted in a given mode are monitored by introducing an artificial two-level system resonant with its frequency (analogous to a Fabry-Perot cavity), has allowed one to extensively explore multiphoton correlations for single emitters [19]. In particular, the potential of virtual transitions, where photons are emitted in bundles, as a source of quantum correlations has been pointed out. As for interacting emitters, the quantum correlations which emerge for two weakly interacting emitters have been investigated in the specific configuration of a pump driving a single emitter, although the fluorescence spectrum is not substantially affected by the interaction in this configuration [20].

Here we investigate two-color photon correlations in the light emitted by two strongly coupled two-level emitters. Spectral filtering allows us to manipulate the light statistics and we show that the resonances induced by dipole-dipole interactions give rise to specific correlations, where the time symmetry of the correlations is broken. To start, in Sec. II, we present our system and the sensor model [18], which allow us to calculate the photon-photon correlation functions. In Sec. III, we present the fluorescence spectrum and the computed photon-photon correlations. We interpret these correlations based on the collective dressed states picture, which encompasses both cases associated with specific resonances and classical correlations, and processes where pairs of

*Corresponding author: darsheshdare@gmail.com
†mathilde.hugbart@inphyni.cnrs.fr
‡bachelard.romain@gmail.com
§celsovb@df.ufscar.br

photons are emitted with nonclassical correlations. Such nonclassicality is witnessed by the violation of Cauchy-Schwatz and Bell inequalities, which is stronger when the system does transit through "virtual" manifolds, also called "leapfrog processes" [21]. Finally, in Sec. IV, we present our conclusions and perspectives.

II. MODELING AND DETECTION SCHEME

In our work, we consider two identical two-level systems. Experimentally, this can be either two atoms, two molecules, or two quantum dots. For this last example, although quantum dots are promising single-emitter platforms, it remains very challenging to produce very similar dots, i.e., with very similar transition frequencies and linewidths. On the other hand, laser cooling has allowed one to bring the interactions between cold atoms under a very high degree of control. In this paper, the two-level system is considered to be a motionless atom.

The system under study is thus composed of two identical driven two-level systems (TLSs) at positions $\mathbf{r}_i$, with transition frequency ω_a and linewidth Γ. Each atom is described by the spin-half angular momentum algebra, with σ_i^- (σ_i^+) the lowering (rising) operator of the ith atom ($i = 1, 2$). In the Born, Markov, and rotating-wave approximations, the master equation which describes the dynamics of its density matrix ρ, in the laser reference frame, is given by [22] ($\hbar = 1$)

$$\frac{\partial \rho}{\partial t} = i[\rho, H] + \mathcal{L}\rho, \tag{1}$$

where the coherent and incoherent parts are encoded in the following Hamiltonian and Lindblad superoperator, respectively:

$$H = \frac{1}{2}\sum_i [\Omega^*(\mathbf{r}_j)\sigma_i^- + \Omega(\mathbf{r}_j)\sigma_i^+] + \Gamma \sum_{i,j\neq i} \delta_{ij}\sigma_i^+\sigma_j^-, \tag{2}$$

$$\mathcal{L}\rho = \frac{\Gamma}{2}\sum_i (2\sigma_i^-\rho\sigma_i^+ - \sigma_i^+\sigma_i^-\rho - \rho\sigma_i^+\sigma_i^-) + \frac{\Gamma}{2}\sum_{i,j\neq i}\gamma_{ij}(2\sigma_j^-\rho\sigma_i^+ - \sigma_i^+\sigma_j^-\rho - \rho\sigma_i^+\sigma_j^-). \tag{3}$$

The atoms here are resonantly driven by a monochromatic plane wave $\Omega(\mathbf{r}) = \Omega e^{i\mathbf{k}_L\cdot\mathbf{r}}$, where Ω stands for the Rabi frequency and $\mathbf{k}_L$ the light wave vector. The dipole-dipole interactions give rise to a coherent and an incoherent coupling,

$$\delta_{ij} = -\frac{3}{4}(1-\cos^2\theta_{ij})\frac{\cos(kr_{ij})}{kr_{ij}} + \frac{3}{4}(1-3\cos^2\theta_{ij})\left[\frac{\sin(kr_{ij})}{(kr_{ij})^2} + \frac{\cos(kr_{ij})}{(kr_{ij})^3}\right],$$

$$\gamma_{ij} = \frac{3}{2}(1-\cos^2\theta_{ij})\frac{\sin(kr_{ij})}{kr_{ij}} + \frac{3}{2}(1-3\cos^2\theta_{ij})\left[\frac{\cos(kr_{ij})}{(kr_{ij})^2} - \frac{\sin(kr_{ij})}{(kr_{ij})^3}\right], \tag{4}$$

with $\lambda = 2\pi/k$ the wavelength transition ($k \approx k_L$), r_{ij} the distance between the atoms, and θ_{ij} the angle between their dipole moments and the vector joining them, $\mathbf{r}_{ij} = \mathbf{r}_j - \mathbf{r}_i$.

Solving the master equation allows one to compute the scattered electric field. For a given polarization (omitted hereafter, for simplicity) and in the far-field limit, the field radiated in direction $\hat{\mathbf{n}}$ is given by

$$E^\dagger(t) = \sum_{j=1}^{2}\sigma_j^-(t)e^{-ik\hat{\mathbf{n}}\cdot\mathbf{r}_j}. \tag{5}$$

The dependence on $\hat{\mathbf{n}}$ is also kept implicit. The field's temporal coherence is captured by the first-order and second-order two-time correlation functions,

$$g^{(1)}(\tau) = \lim_{t\to\infty}\frac{\langle E(t)E^\dagger(t+\tau)\rangle}{\langle E(t)E^\dagger(t)\rangle}, \tag{6}$$

$$g^{(2)}(\tau) = \lim_{t\to\infty}\frac{\langle E(t)E(t+\tau)E^\dagger(t+\tau)E^\dagger(t)\rangle}{\langle E(t)E^\dagger(t)\rangle^2}, \tag{7}$$

here computed in the steady state. In particular, the fluorescence spectrum, sometimes referred to as the one-photon spectrum, is obtained from the Fourier transform of the first-order correlation function,

$$S(\omega) = \lim_{T\to\infty}\int_{-T}^{T} g^{(1)}(\tau)e^{-i\omega\tau}d\tau. \tag{8}$$

The one-photon spectrum gives the spectral energy distribution of the light scattered elastically and inelastically, whereas the second-order correlation function $g^{(2)}$ contains details of the correlations between the emitted photons, with the antibunching in the trains of photons emitted by a single emitter as a hallmark of the nonclassicality of this emission [23].

The problem of time-resolved observables is, however, more challenging. Indeed, as one introduces the field operator in the reciprocal space, $\tilde{E}(\omega) = \int_{t=-\infty}^{\infty} e^{-i\omega t}E(t)dt$, the problem of studying two-color photon-photon correlations brings in the calculation of a four-time correlator, $\langle E(t_1)E(t_2)E^\dagger(t_3)E^\dagger(t_4)\rangle$. Then, the use of the quantum regression theorem, commonly used for two-time observables, becomes a daunting task [24–26]. This is a strong restriction to the study of photon-photon correlations, which has long limited rigorous results to single-emitter physics [27].

An elegant solution was found in the "sensor method" that allows one to theoretically investigate frequency-resolved correlations in greater detail [18]. It relies on the introduction in the system of extra two-level systems which behave as sensors, as described by the Hamiltonian

$$H_S = \sum_s \omega_s\xi_s^\dagger\xi_s^- + \varepsilon\sum_s\left(E\xi_s^- + E^\dagger\xi_s^\dagger\right), \tag{9}$$

with ξ_s ($\xi_s^\dagger$) the lowering (rising) operator for sensor s, and ω_s its resonant frequency, in the rotating frame at the laser frequency [28]. The ε parameter corresponds to the coupling strength between the sensors and the atomic system, which must be made sufficiently small to not significantly perturb the dynamics of the latter and to avoid the saturation of the sensor ($\varepsilon = 10^{-4}$ throughout the paper). The sensors are also characterized by their linewidth Γ_s, a parameter of importance as we shall see later, which manifests in an extra

Lindblad term,

$$\mathcal{L}_S\rho = \frac{\Gamma_s}{2}\sum_s (2\xi_s^- \rho \xi_s^\dagger - \xi_s^\dagger \xi_s^- \rho - \rho \xi_s^\dagger \xi_s^-). \quad (10)$$

The sensor contributions (9),(10) are then added to the master equation (1), with ρ now describing the density matrix of the whole system (atoms plus sensors).

The steady-state two-photon time- and frequency-resolved correlation is then obtained from the second-order correlation function from the sensors operators,

$$g_s^{(2)}(\omega_1, \omega_2, \tau) = \lim_{t\to\infty} \frac{\langle \xi_1^\dagger(\omega_1, t)\xi_2^\dagger(\omega_2, t+\tau)\xi_2(\omega_2, t+\tau)\xi_1(\omega_1, t)\rangle}{\langle \xi_1^\dagger(\omega_1, t)\xi_1(\omega_1, t)\rangle \langle \xi_2^\dagger(\omega_2, t)\xi_2(\omega_2, t)\rangle}. \quad (11)$$

Equal-time correlations ($\tau = 0$) characterize the simultaneous emission of photons of frequencies ω_1 and ω_2; they are hereafter called two-photon frequency-resolved correlations and noted by $g_s^{(2)}(\omega_1, \omega_2)$, for simplicity. Thus, at the expense of two extra degrees of freedom, equal-time frequency-resolved correlations $g_s^{(2)}(\omega_1, \omega_2)$ are contained in the steady-state values of the density matrix, while time- and frequency-resolved ones [i.e., $g_s^{(2)}(\omega_1, \omega_2, \tau)$] are obtained as two-time correlators, using the "standard" (two-time) quantum regression theorem [29].

Experimentally, frequency-resolved signals can be obtained using frequency filters such as Fabry-Perot cavities with resonance frequency and linewidth of the sensors, ω_s and Γ_s, but also from time-resolved measurements using beatnote techniques for the $g^{(1)}(\tau)$ function [30,31], for example. Throughout this work, the correlation functions were computed using the QUTIP toolbox [32,33] and the MATLAB software, using a solver to reach the steady state.

III. STRONGLY INTERACTING ATOMS

A. Fluorescence spectrum

The radiation spectrum of a strongly driven two-level emitter has a rather intuitive interpretation in the dressed state picture: after the light modes were traced out to obtain Eqs. (2) and (3) [9,10], in this picture the photon number is restored to obtain hybrid atom-field states. The resulting atom-field eigenstates have been discussed extensively for single emitters [34], and the coupling of light to the atom leads to the following eigenstates for the Hamiltonian at resonance:

$$|\pm\rangle = \frac{1}{\sqrt{2}}(|\uparrow, n-1\rangle \pm |\downarrow, n\rangle), \quad (12)$$

where $|\downarrow\rangle$ and $|\uparrow\rangle$ denote the single-atom ground and excited states, respectively, and n is the photon number in the driving field (i.e., the laser). This pair of eigenstates forms the n-excitation manifold: in each manifold, the eigenstates are split by the Rabi frequency of the driving field (unless the cavity quantum electrodynamics regime is reached [35,36]).

For a pair of atoms, the dipole-dipole interaction in Eqs. (2) and (3) generates two collective single-excitation eigenstates, labeled symmetric and antisymmetric,

$$|S\rangle = (|\uparrow\downarrow\rangle + |\downarrow\uparrow\rangle)/\sqrt{2},$$

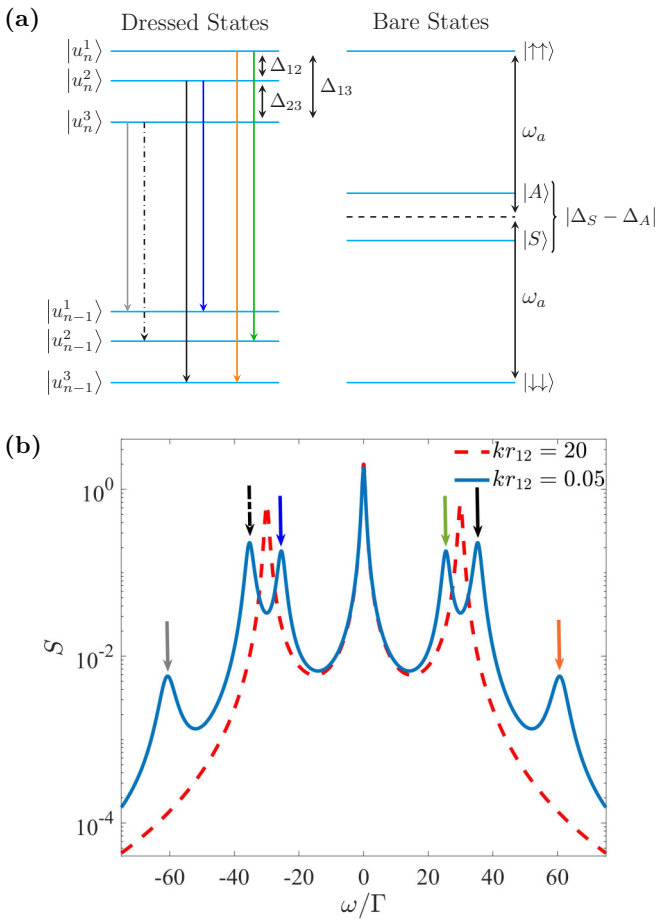

FIG. 1. (a) Collective dressed (left) and bare (right) states for two strongly interacting atoms, in the rotating frame of the laser and in the laboratory frame, respectively. (b) Spectrum of two interacting atoms. The colored arrows above the peaks (of the solid blue line) correspond to the transitions depicted in (a). Simulations carried out for two atoms driven with a field of Rabi frequency $\Omega = 30\Gamma$, with dipole orientation $\theta_{12} = \cos^{-1}(1/\sqrt{3})$, and separated by a distance $kr_{12} = 0.05$ (solid blue line) and $kr_{12} = 20$ (dashed red line).

$$|A\rangle = (|\uparrow\downarrow\rangle - |\downarrow\uparrow\rangle)/\sqrt{2}, \quad (13)$$

which present linewidths $\Gamma_S = \Gamma(1+\gamma_{12})$ and $\Gamma_A = \Gamma(1-\gamma_{12})$, and energy shifts $\Delta_S = \Gamma\delta_{12}$ and $\Delta_A = -\Gamma\delta_{12}$. Throughout this work, we have fixed $\cos(\theta_{12}) = 1/\sqrt{3}$, which implies $\delta_{12} < 0$ for the interatomic distances considered and, consequently, $\Delta_S < \Delta_A$, as shown in Fig. 1. The choice of the θ_{12} angle is somewhat arbitrary since we can obtain the same results for the photon statistics for other angles, as long as we properly adjust the dipoles' orientation (using, e.g., an external magnetic field) and the relative position between the emitters. The important parameter here is the effective couplings (coherent and incoherent) between the two two-level emitters, which depend on both the relative position and the angle θ_{12}.

Here we consider the case of two very close, strongly interacting atoms ($kr_{12} \ll 1$ or, more specifically, $|\delta_{12}| \gg 1$ and $\gamma_{12} \approx 1$), in the presence of a strong resonant driving, char-

acterized by $\Omega^2 > \Gamma^2 + 4|\Gamma\delta_{12}|^2$. Following the approach of Ref. [34], we consider the following basis:

$$|\phi_n^1\rangle = |\uparrow\uparrow, n-2\rangle, \tag{14a}$$

$$|\phi_n^2\rangle = |S, n-1\rangle, \tag{14b}$$

$$|\phi_n^3\rangle = |A, n-1\rangle, \tag{14c}$$

$$|\phi_n^4\rangle = |\downarrow\downarrow, n\rangle, \tag{14d}$$

which is the four-dimensional subspace of the eigenvectors of the operator $N_T = N_v + 1/2 + \sum_{i=1,2}(1 + \sigma_i^+\sigma_i^-)/2$, where N_v is the photon number operator for eigenvalue n. In this basis, the eigenstates of the atom-light system are composed of the collective dressed states incorporating the eigenstates of Hamiltonian (2) for two atoms with light-mediated interactions, and the photon number states of the light field i.e., the n-excitation manifold for our system is given by

$$|u_n^1\rangle = a_1|\uparrow\uparrow, n-2\rangle + a_2\sqrt{2}|S, n-1\rangle + a_1|\downarrow\downarrow, n\rangle, \tag{15a}$$

$$|u_n^a\rangle = |A, n-1\rangle, \tag{15b}$$

$$|u_n^2\rangle = -\frac{1}{\sqrt{2}}|\uparrow\uparrow, n-2\rangle + \frac{1}{\sqrt{2}}|\downarrow\downarrow, n\rangle, \tag{15c}$$

$$|u_n^3\rangle = a_2|\uparrow\uparrow, n-2\rangle - a_1\sqrt{2}|S, n-1\rangle + a_2|\downarrow\downarrow, n\rangle, \tag{15d}$$

where we have introduced

$$a_1 = -v_1/\sqrt{2+2v_1^2}, \tag{16a}$$

$$a_2 = 1/\sqrt{2+2v_1^2}, \tag{16b}$$

$$v_1 = -\frac{4(kr_{ij})^2\Omega^2 + \cos(kr_{ij})c + \cos^2(kr_{ij})}{(kr_{ij})\Omega[c + 3\cos(kr_{ij})]}, \tag{16c}$$

$$c = \sqrt{16(kr_{ij})^2\Omega^2 + \cos^2(kr_{ij})}. \tag{16d}$$

These dressed states are characterized by an entanglement between the atomic and field states, apart from the one containing the antisymmetric atomic state, $|u_n^a\rangle$. Since the latter state is not entangled with the field states, nor is it coupled to the other states through the Hamiltonian, it does not participate in the dressing. Furthermore, in the limit of strong coupling of the atoms considered here, it can be shown that this antisymmetric state does not participate substantially in the steady-state fluorescence spectrum. Although it is not driven directly by the laser ($kr_{12} \ll 1$ leads to a rather homogeneous phase profile of the laser on the atoms, thus addressing the symmetric state), it gets substantially populated by decay from the atomic state $|\uparrow\uparrow\rangle$ and its long lifetime allows it to hold a substantial population [37]. Nevertheless, the weak linewidth also translates into a low number of emitted photons. Thus, unless specified (see Sec. III B), we hereafter neglect this state in our analysis.

Neglecting the asymmetric state leads us to introduce the collective operator $\sigma_S^{+-} = (\sigma_1^{+-} + \sigma_2^{+-})/\sqrt{2}$ and simplify the Lindbladian (3) into $\mathcal{L}_{\sigma_S}\rho = \Gamma_S(2\sigma_S^-\rho\sigma_S^+ - \sigma_S^+\sigma_S^-\rho - \rho\sigma_S^+\sigma_S^-)$ in the strong interaction regime. As a consequence, the n-excitation manifold reduces to the triplet of $(|u_n^1\rangle, |u_n^2\rangle, |u_n^3\rangle)$, with the frequency difference

$$\Delta_{ij} = -\Delta_{ji} \equiv E_n^i - E_n^j. \tag{17}$$

The dressed energy levels are then composed of the n-excitation manifolds, each composed of the above triplet, and with successive manifolds separated by energy ω_L: the dressed states and the equivalent bare collective energy levels for two interacting atoms are presented in Fig. 1(a). The one-photon spectrum is obtained by solving the master equation from Eqs. (1)–(3) combined with the quantum regression theorem or, equivalently, monitoring the population of a sensor whose resonant frequency ω_s is tuned. The fluorescence spectrum for two strongly interacting atoms is depicted in Fig. 1(b) ($kr = 0.05$, solid blue line), where the different peaks can be interpreted in the dressed state picture. Similarly to the single-atom case, the central peak originates in the $|u_n^i\rangle \to |u_{n-1}^i\rangle$ transitions ($i = 1, 2, 3$), which do not alter the atomic state and are characterized by the emission of a photon at the laser frequency ω_L. For comparison, in Fig. 1(b), we also plot the fluorescence spectrum for two weakly interacting atoms ($kr = 20$, red dashed line), which is extremely similar to the single-atom spectrum.

The transformation of the doublet of states into a triplet of states for the n-excitation manifold, due to the interactions, leads to a seven-peak spectrum. The six sidebands are collective, corresponding to resonant frequencies $\pm\Delta_{ij}$ not present for single atoms (all transitions are hereafter given in the laser frame), and the corresponding transitions $|u_n^i\rangle \to |u_{n-1}^{j\neq i}\rangle$ are presented schematically in the dressed state picture of Fig. 1(a).

B. Photon-photon correlations

Let us now study the specific correlations which occur between these different emission processes. While the transitions from one manifold to the next are the origin of the one-photon spectrum, the correlations in the emitted photons are the essence of the two-photon frequency-resolved correlations, $g_s^{(2)}(\omega_1, \omega_2)$, computed using Eq. (11). The two-photon frequency-resolved correlations corresponding to the situation of Fig. 1 are presented in Fig. 2(a), the complexity of which reflects the diversity in photon-photon correlations. For the sake of comparison, in Fig. 3 we plot steady-state photon-photon correlations $g_s^{(2)}(\omega_1, \omega_2)$ for (a) a single atom, (b) two atoms separated by $kr = 20$ (i.e., the interaction is negligible), and (c) two close atoms, with $kr = 0.4$. For two remote atoms ($kr = 20$), the two-photon correlation function is close to the single-atom case, yet with less contrast since each atom can emit independently.

Opposite-sideband correlations. We first discuss the correlation between opposite sidebands, i.e., with frequency $+\Delta_{ij}$ and $-\Delta_{ij}$, as shown by the • symbol for $(i, j) = (1, 2)$ in Fig. 2(a): it corresponds to the two-photon cascade $|u_n^1\rangle \to |u_{n-1}^2\rangle \to |u_{n-2}^1\rangle$, shown in Fig. 2(b). Being an allowed path of relaxation, it leads to photon-photon bunching, $g_s^{(2)}(\Delta_{12}, -\Delta_{12}) > 1$: this case is similar to the opposite-sideband bunching effect reported for single emitters [6,7]. The same holds true for other transitions of the form $|u_n^i\rangle \to |u_{n-1}^j\rangle \to |u_{n-2}^i\rangle$, corresponding to the other sidebands.

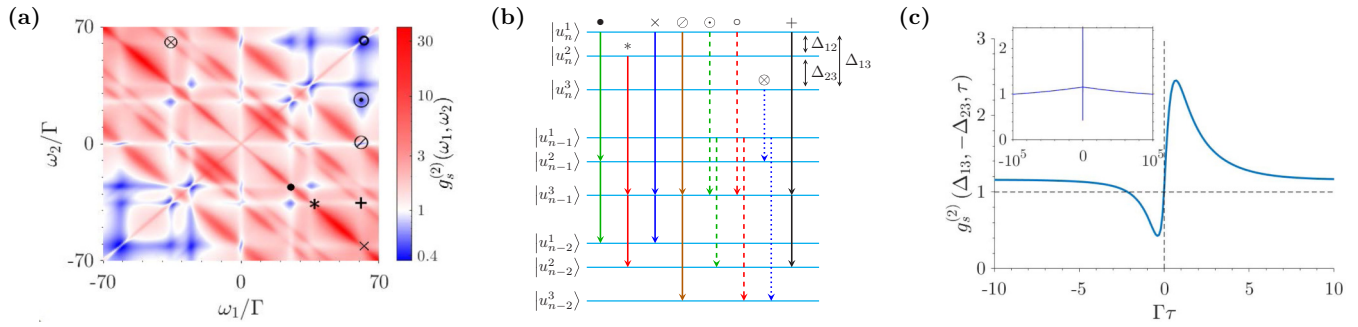

FIG. 2. (a) Steady-state photon-photon correlations $g_s^{(2)}(\omega_1, \omega_2)$ for a pair of strongly interacting, strongly driven atoms. (b) Cascade processes involving the emission of two photons, according to the energy levels of the dressed states picture (allowed cascades with solid lines, forbidden processes with dashed/dotted ones; see text). The associated $g_s^{(2)}(\omega_1, \omega_2)$ is given by the same symbols in (a). Simulations realized for two atoms with (a) $kr_{12} = 0.05$, $\theta_{12} = \cos^{-1}(1/\sqrt{3})$, $\Omega = 30\Gamma$, and $\Gamma_s = \Gamma$. (c) Time-resolved $g_s^{(2)}(\omega_1, \omega_2, \tau)$ for the transitions involving photons of frequency $(\omega_1, \omega_2) = (\Delta_{13}, -\Delta_{23})$ [+ symbol in (a) and (b)] with $\Gamma_s = \Gamma$. Inset: same curve, for a broader time window. Simulations realized for two atoms with $kr = 0.006$, $\theta = \cos^{-1}(1/\sqrt{3})$, $\Omega = 250\Gamma$, and $\Gamma_s = 5\Gamma$.

Equal-sideband correlations. Photons emitted from the same sidebands come antibunched, as in all cases the associated relaxation path is blocked (as long as there is no degeneracy, i.e., $\Delta_{12} \neq \Delta_{23}$). An analogous effect is observed for single atoms. For instance, a photon of frequency Δ_{13} automatically leads the system to state $|u_{n-1}^3\rangle$, so the next photon cannot be emitted at the same frequency as it requires for the system to be in a state $|u_{n-1}^1\rangle$ (states $|u_{n-1}^1\rangle$ and $|u_{n-1}^3\rangle$ are orthogonal). For this reason, the associated path of relaxation is considered blocked [see the ∘ symbol cascade in Fig. 2(b)], and it is characterized by antibunched photons: $g_s^{(2)}(\Delta_{13}, \Delta_{13}) < 1$ [∘ symbol in Fig. 2(a)].

Nevertheless, as can be seen in Fig. 2(a), photons from the same sidebands suffer from being in the "indistinguishability bunching line" of the two-photon frequency-resolved correlations. Indeed, two photons with the same frequency cannot be distinguished by the sensor, which, in turn, leads to bunching effects. This manifests in the "overbunched" diagonal line in Fig. 2(a).

Cross-sideband correlations. Let us now discuss processes which involve photons from two different sidebands, corresponding to $g_s^{(2)}(\pm\Delta_{ij}, \pm\Delta_{i'j'})$ with $(i, j) \neq (i', j')$. For these processes which involve the three states (15a), (15c), and (15d), a more careful analysis is needed, as photons of different frequencies may be emitted in a specific order. For instance, the double transition $|u_n^1\rangle \to |u_{n-1}^3\rangle \to |u_{n-2}^2\rangle$, indicated by a + symbol in the dressed state representation of Fig. 2(b), is allowed, and thus permits the successive emission of photons of frequency Δ_{13} and $-\Delta_{23}$, in that order. But a photon of frequency $-\Delta_{23}$ cannot be followed by one of frequency Δ_{13} since this would correspond to the successive $|u_n^3\rangle \to |u_{n-1}^2\rangle$ and $|u_{n-1}^1\rangle \to |u_{n-2}^3\rangle$ [see ⊗ symbol in Fig. 2(b)], which is a blocked path since $|u_{n-1}^2\rangle$ and $|u_{n-1}^1\rangle$ are orthogonal.

Monitoring the zero-delay photon-photon correlations $g_s^{(2)}(\Delta_{ij}, \Delta_{i'j'})$ does not allow one to distinguish the two processes, but its time-resolved version does. As illustrated by the computation of $g_s^{(2)}(\Delta_{13}, -\Delta_{23}, \tau)$ in Fig. 2(c), we observe a strong bunching at delays $\tau \sim +1/\Gamma$, but a below-unity $g_s^{(2)}$ for $\tau \sim -1/\Gamma$ [negative times corresponds to the reverse order since $g_s^{(2)}(\Delta_{13}, -\Delta_{23}, \tau) = g_s^{(2)}(-\Delta_{23}, \Delta_{13}, -\tau)$]. The same phenomenon is observed for transitions with photon pairs of frequency $(\pm\Delta_{12}, \mp\Delta_{13})$ and $(\pm\Delta_{12}, \pm\Delta_{23})$. Thus, these double transitions, which involve the three different atomic states, present a time-symmetry breaking for the $g_s^{(2)}$ function, which corresponds to a specific ordering of the emitted photons. It is due to the interaction between the emitters, which leads to a splitting of the energy levels of the atomic system.

It is interesting to note that on timescales τ of several single-atom excited state lifetimes, the correlator $g_s^{(2)}(\Delta_{13}, -\Delta_{23}, \tau)$ does not go to 1 as one would expect: this

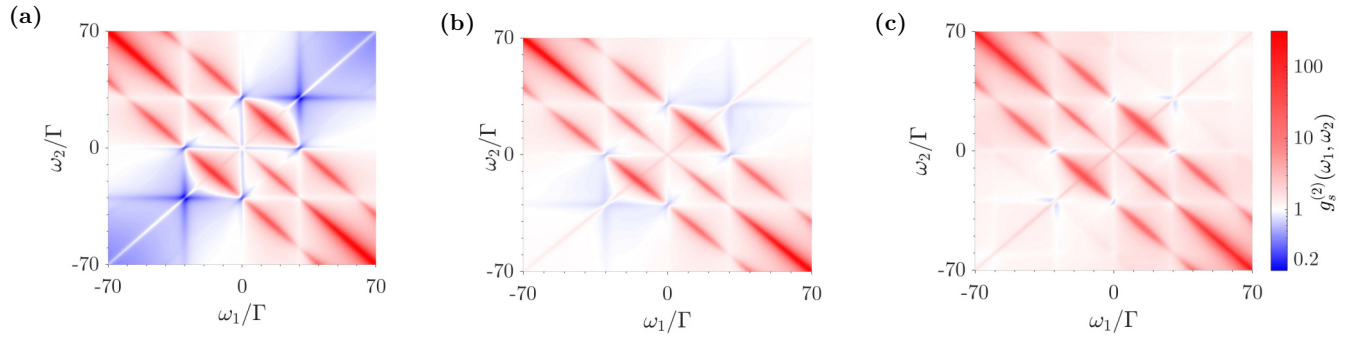

FIG. 3. Steady-state photon-photon correlations $g_s^{(2)}(\omega_1, \omega_2)$, for comparison with Fig. 2(a), for (a) a single atom, and for two interacting atoms with (b) $kr = 20$, and (c) $kr = 0.4$. Simulations realized for $\Omega = 30\Gamma$, $\Gamma_s = \Gamma$, and $\theta = \cos^{-1}(1/\sqrt{3})$ (two-atom cases).

is the signature of the antisymmetric state holding a substantial part of the atomic excitations, yet these are released on the mode timescale [37] [see inset of Fig. 2(c)].

Finally, the case of double processes that depart twice from the same atomic state, but go to the two other atomic states (i.e., $|u_n^i\rangle \to |u_{n-1}^j\rangle$ and $|u_{n-1}^i\rangle \to |u_{n-2}^l\rangle$, with i, j, and l all different), are naturally antibunched. Indeed, both possible orders for the double transition are blocked. Consequently, $g_s^2(\Delta_{ij}, \Delta_{il})$ is below unity, as can be observed in Fig. 2(a) (see the $\odot$ symbol).

Sideband-central peak correlations. Finally, cascades which involve one sideband photon plus a central peak photon can, in principle, occur successively since the latter does not involve a change in the atomic state (i.e., $|u_n^i\rangle \to |u_{n-1}^i\rangle$). Furthermore, both orders of emission for the photons could equally occur. Nonetheless, these pairs of photons come antibunched. As discussed for the case of single emitters [38], this effect originates from a destructive interference, due to the fact that the state of the system is not modified by Rayleigh emission. Thus, despite the two cascades involving photons of relative frequency (in the rotating frame of the laser field), Δ_{ij} and 0 are degenerate (they have the same initial and final states), and the interference between the amplitude of their transition probability prevents the process instead of favoring it [see Fig. 2(a)].

Finally, we point out that a clear observation of antibunching, and other kinds of photon-photon correlations as we investigate in this paper, requires the use of sensors of linewidth at least comparable to the atomic linewidth (here they are taken to be equal: $\Gamma_s = \Gamma$). Indeed, it has recently been shown that antibunching (and other photon-photon correlations), even in the temporal domain [39–41] [as given by $g^{(2)}(\tau)$], is strongly reduced in the case of a sublinewidth filtering since it results in long integration time, which in turn averages out the correlations [42].

C. Leapfrog processes

The cascades described above involve two-photon emission processes that encompass real transitions through intermediate states, where the system state is described by the manifolds from the dressed atom picture. There exist other kinds of two-photon transitions, where the system does not transit through one of these intermediate states, but rather through a "virtual" manifold, labeled "leapfrog processes" [21]. These transitions are characterized by the joint emission of two photons and have recently been observed in single quantum dots [43]. Most of these two-photon collective processes yield correlations much stronger than (cascade) resonant transitions, and their quantum nature has been demonstrated for single emitters using Cauchy-Schwarz and Bell inequalities [42].

For these leapfrog processes, the energy of each photon does not need to be related to a specific level transition energy, only their sum needs to obey the relation

$$\omega_1 + \omega_2 = 0, \ \pm\Delta_{ij} \tag{18}$$

(the frequency in the laboratory frame is obtained by adding $2\omega_L$). The leapfrog transitions correspond to the antidiagonal lines marked by color arrows (green, black, and orange) in Figs. 4(b) and 4(c), and the associated (virtual) transitions are depicted in Fig. 4(a). Note that if, in addition to condition (18), the energy of each photon belongs to the allowed resonant transitions, the photon emission process is that described in the previous section and the correlations between the photons are classical.

To characterize the nonclassicality of these correlations, we use the Cauchy-Schwarz inequality (CSI) for the second-order correlation functions at zero delay $g_{kl}^{(2)} = g_s^{(2)}(\omega_k, \omega_l)$,

$$\left[g_{12}^{(2)}\right]^2 \leqslant g_{11}^{(2)} g_{22}^{(2)}, \tag{19}$$

which we monitor by studying the ratio

$$R_s = \frac{\left[g_{12}^{(2)}\right]^2}{g_{11}^{(2)} g_{22}^{(2)}}. \tag{20}$$

Values R_s larger than unity are the signatures of nonclassical correlations between the two emitted photons [42]. Figure 4(b) shows the CSI violations for two strongly interacting atoms. In order to show more explicitly how different two-photon correlations are in the strongly interacting case, as compared to the single-atom and to the weakly interacting atom cases, we plot in Fig. 5 the ratio R_s for different configurations: (a) for a single atom, and for two atoms [with dipole orientation $\theta = \cos^{-1}(1/\sqrt{3})$] separated by (b) $kr = 20$ and (c) $kr = 0.4$. We note that for $kr \gtrsim 1$, R_s essentially behaves like in the single-atom case. Differently, for $kr = 0.4$, new antidiagonal lines start to appear, although no strong correlations result from them (Fig. 3) and no CSI violation is observed in these lines [Figs. 5(c) and 6(c)].

In Fig. 4(a), leapfrog processes which involve different initial and final atomic states are presented: the system does not emit photons from specific ("real") transitions, only the sum of the two-photon energies corresponds to a transition between specific states in the dressed states picture. As one can observe from the antidiagonal lines in Fig. 4(b), which correspond to $\omega_1 + \omega_2 = 0, \ \pm\Delta_{ij}$, the Cauchy-Schwarz inequality is violated for most of these joint emission processes ($R_s > 1$). Nevertheless, the Cauchy-Schwarz inequality is not violated for antibunched resonant transitions, i.e., for photon pairs with frequencies $(0, \pm\Delta_{ij})$ or $(\pm\Delta_{ij}, 0)$ [see, for example, symbol $\oslash$ for frequencies $(\Delta_{13}, 0)$]. Neither is it violated for pairs of real photons, for frequencies $(\pm\Delta_{12}, \pm\Delta_{23})$. Also, as we can observe in Figs. 6(a) and 6(b), a sublinewidth filtering leads to weaker violations of Cauchy-Schwarz inequality [42].

Finally, one observes that the inequality is also violated for some emission processes which involve real transitions, where the correlations between emitted photons are classical [see the $+$ or $\otimes$ symbols, for example, in Fig. 4(b)]. In order to properly observe the classicality of these correlations, as they correspond to photons of real transitions located in the leapfrog lines, it is necessary to use a sensor with a better resolution. Indeed, the use of a sensor linewidth $\Gamma_s = \Gamma$ leads to an averaging over processes with different kinds of correlations. To illustrate this point, we show in Fig. 6(a) the change in Cauchy-Schwarz inequality as the sensor linewidth is changed from Γ to $\Gamma/10$: the above-mentioned transitions for the photons from resonant transitions do not violate any Cauchy-Schwarz inequality, showing the classical nature of their correlations [42].

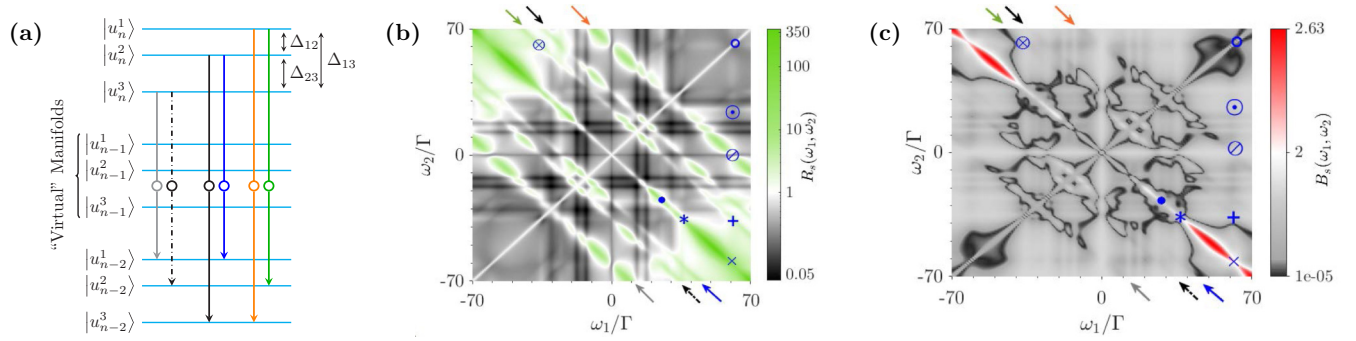

FIG. 4. (a) Two-photon "leapfrog" processes, with the system transiting through virtual dressed levels. (b) Ratio R_s from the Cauchy-Schwarz inequality, and (c) B_s from the Bell inequality, when tuning the frequency of each sensor. Simulations realized for $kr = 0.05$, $\theta = \cos^{-1}(1/\sqrt{3})$, $\Omega = 30\Gamma$, and $\Gamma_s = \Gamma$.

Furthermore, as for single emitters [42], violations of Cauchy-Schwarz inequality may appear for transitions of the central antidiagonal line ($\omega_1 + \omega_2 = 0$), even for real transitions and for well-resolved frequencies: Fig. 6(b) presents such violations of Cauchy-Schwarz inequality (see the •, ∗, and × symbols). This failure of Cauchy-Schwarz inequality to detect classical correlations can be addressed by using the Bell inequality (BI), as monitored by a quantifier adapted to the sensor approach [42],

$$B_s = \sqrt{2}\left|\frac{B_{1111} + B_{2222} - 4B_{1221} - B_{1122} - B_{2211}}{B_{1111} + B_{2222} + 2B_{1221}}\right|, \quad (21)$$

with $B_{jklm} = \langle \xi_1^\dagger(\omega_j)\xi_2^\dagger(\omega_k)\xi_2(\omega_l)\xi_1(\omega_m)\rangle$. Values $B_s > 2$ are a violation of the BI, which are considered as a true signature of quantum correlations. As can be seen in Fig. 4(c) for $\Gamma_s = \Gamma$, Bell inequalities are violated only for specific areas of the central antidiagonal line, yet not for the real transitions of • and ∗. This behavior is similar to the single-emitter case [42], confirming that only transitions involving virtual states hold true quantum correlations between the emitted photons. Note that the Bell inequality and Cauchy-Schwarz inequality are sensitive to the frequency resolution of the sensors, as narrow linewidth sensors correspond to long averaging time, which in turn washes out the correlations [42].

As illustrated for the pair of photons $(\pm\Delta_{13}, \mp\Delta_{13})$, a sensor linewidth $\Gamma_s = \Gamma$ presents a violation of BI, yet reducing the sensor linewidth to $\Gamma/10$ removes the violation of the BI; see Fig. 6(d), where the pair of $(\Delta_{13}, -\Delta_{13})$ is indicated by ×. This again highlights that the narrow linewidth sensors correspond to a finer structure for the quantum quantifiers and the necessity of using sensors with a linewidth comparable to the atomic transition one, in order to detect the stronger correlations. Differently, the sidebands which rise directly from the interaction, at $\omega_1 + \omega_2 = 2\Omega$, do not present signatures of nonclassicality, as illustrated in Fig. 6(c).

IV. CONCLUSION AND PERSPECTIVES

Strong interactions between two two-level emitters give rise to a series of new sidebands in the fluorescence spectrum, whose shift from the atomic transition depends on both the interaction strength and the driving field. Similarly to the single emitters, the leapfrog processes with frequencies that sum to zero or the frequency of one of the interaction-induced sidebands are characterized by strong correlations, which can be either classical or quantum. This suggests that strongly coupled emitters are potential sources of heralded photons, with extra control parameters through the interaction, as compared to single emitters.

Another regime of interest is that of a weak dipole-dipole interaction, i.e., when the collective dressed levels are equally spaced in energy ($\Delta_{12} = \Delta_{23}$), which occurs when the distance between the emitters is comparable or larger than the optical wavelength. In this regime, the first correction to the single-atom fluorescence spectrum is the emergence of

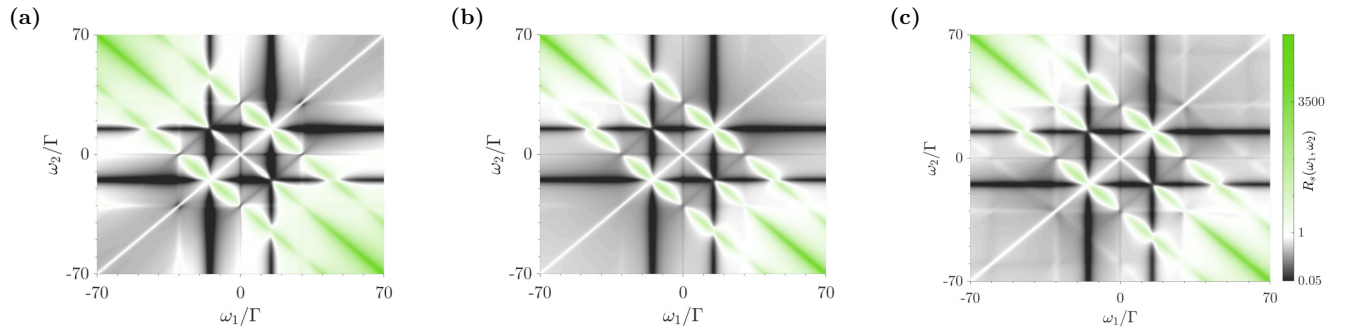

FIG. 5. Ratio R_s from the Cauchy-Schwarz inequality when tuning the frequency of each sensor, for comparison with Fig. 4(b), for (a) a single atom, and for two interacting atoms with $\theta = \cos^{-1}(1/\sqrt{3})$ and (b) $kr = 20$ and (c) $kr = 0.4$. Simulations are realized for $\Omega = 30\Gamma$ and $\Gamma_s = \Gamma$.

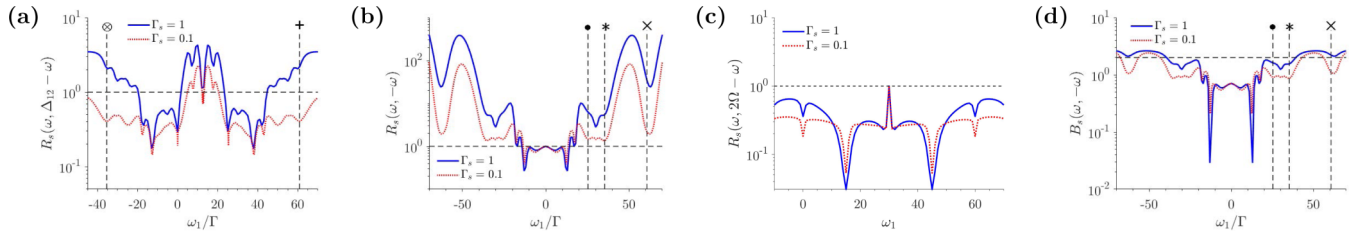

FIG. 6. Quantifier R_s for the Cauchy-Schwarz inequalities (with a violation above the dashed line) for $\Gamma_s = \Gamma$ (solid blue) and $\Gamma_s = \Gamma/10$ (dotted red), for the leapfrog lines (a) $\omega_1 + \omega_2 = \Delta_{12}$, (b) $\omega_1 + \omega_2 = 0$, and (c) $\omega_1 + \omega_2 = 2\Omega$. (d) Quantifier B_s for the Bell inequalities (with a violation above the dashed line) for $\Gamma_s = \Gamma$ (solid blue) and $\Gamma_s = \Gamma/10$ (dotted red) in the leapfrog line of $\omega_1 + \omega_2 = 0$. The vertical lines with a symbol at the top refer to the processes discussed in Figs. 2(a), 4(b) and 4(c). In (c), we show that collective leapfrog lines for two atoms with $kr = 0.4$ do not show a CSI violation as a signature of single-atom physics domination. Simulations realized for $\theta = \cos^{-1}(1/\sqrt{3})$ and $\Omega = 30\Gamma$, in (a),(b),(d) $kr = 0.05$ and (c) $kr = 0.4$.

sidebands shifted from the laser frequency by twice the Rabi frequency ($\omega = \pm 2\Omega$). This phenomenon was predicted to scale with the resonant optical depth for dilute extended clouds, as a signature of the raising two-atom quantum correlations [14]. We have investigated photon-photon correlations $g^{(2)}(\omega_1, \omega_2)$ for a pair of atoms at a distance of the order of λ [$kr = 0.4 - 1$ and $\theta = \cos^{-1}(1/\sqrt{3})$] and strongly driven, yet photon-photon correlations appear to be largely dominated by single-atom physics. This is reminiscent of the antibunching phenomenon which vanishes for a large number of independent emitters, unless specific conditions for their interference is achieved [44]. Furthermore, the leapfrog processes associated with the new sidebands, $\omega_1 + \omega_2 = \pm 2\Omega$, present no violation of the Cauchy-Schwarz inequality [see Fig. 6(c)]. This suggests that although these sidebands result from correlations between the quantum fluctuations of the two dipoles [14], the photons associated with these processes may be only classically correlated.

The variety of sidebands and photon-photon correlations encountered for a pair of atoms calls for a dedicated study for larger systems. Indeed, although the coherent manipulation of atoms at scales below the diffraction limit is experimentally challenging, schemes have been proposed to surpass these limitations, based on the transparency-induced dark states [45–48], which have already allowed for the generation of subwavelength cold atom structures [49–52]. In this context, strongly interacting cold atom ensembles may be a promising tunable source for entangled pairs of photons, but also for larger bunches of photons [19].

ACKNOWLEDGMENTS

M.H., R.B., and C.J.V.-B. acknowledge funding from the French National Research Agency (Projects No. PACE-INANR19-QUAN-003-01 and No. QuaCor ANR19-CE47-0014-01). E.D., R.B., and C.J.V.-B. benefited from grants from the São Paulo Research Foundation (FAPESP, Grants No. 2018/10813-2, No. 2018/01447-2, No. 2018/15554-5, No. 2019/13143-0, and No. 2019/11999-5) and from the National Council for Scientific and Technological Development (CNPq, Grants No. 302981/2017-9, No. 409946/2018-4, and No. 307077/2018-7). M.H. and R.B. received support from the project CAPES-COFECUB (Grant No. Ph879-17/CAPES 88887.130197/2017-01).

[1] G. S. Agarwal, in *Springer Tracts in Modern Physics*, edited by G. Höhler (Springer, Berlin, 1974), pp. 1–128.
[2] B. R. Mollow, Phys. Rev. **188**, 1969 (1969).
[3] A. Aspect, G. Roger, S. Reynaud, J. Dalibard, and C. Cohen-Tannoudji, Phys. Rev. Lett. **45**, 617 (1980).
[4] C. Cohen-Tannoudji, S. Reynaud, R. K. Bullough, and J. M. Vaughan, Philos. Trans. R. Soc. A **293**, 223 (1979).
[5] J. Dalibard and S. Reynaud, J. Phys. **44**, 1337 (1983).
[6] C. A. Schrama, G. Nienhuis, H. A. Dijkerman, C. Steijsiger, and H. G. M. Heideman, Phys. Rev. A **45**, 8045 (1992).
[7] A. Ulhaq, S. Weiler, S. M. Ulrich, R. Roßbach, M. Jetter, and P. Michler, Nat. Photon. **6**, 238 (2012).
[8] S. Wolf, S. Richter, J. von Zanthier, and F. Schmidt-Kaler, Phys. Rev. Lett. **124**, 063603 (2020).
[9] R. H. Lehmberg, Phys. Rev. A **2**, 883 (1970).
[10] R. H. Lehmberg, Phys. Rev. A **2**, 889 (1970).
[11] I. R. Senitzky, Phys. Rev. Lett. **40**, 1334 (1978).
[12] G. S. Agarwal, R. Saxena, L. M. Narducci, D. H. Feng, and R. Gilmore, Phys. Rev. A **21**, 257 (1980).
[13] Y. Ben-Aryeh and C. M. Bowden, IEEE J. Quantum Electron. **24**, 1376 (1988).
[14] L. Pucci, A. Roy, T. S. do Espirito Santo, R. Kaiser, M. Kastner, and R. Bachelard, Phys. Rev. A **95**, 053625 (2017).
[15] N. Gisin, G. Ribordy, W. Tittel, and H. Zbiden, Rev. Mod. Phys. **74**, 145 (2002).
[16] E. Polino, M. Valeri, N. Spagnolo, and F. Sciarrino, AVS Quantum Sci. **2**, 024703 (2020).
[17] A. Zeilinger, Rev. Mod. Phys. **71**, S288 (1999).
[18] E. del Valle, A. Gonzalez-Tudela, F. P. Laussy, C. Tejedor, and M. J. Hartmann, Phys. Rev. Lett. **109**, 183601 (2012).
[19] J. C. L. Carreño, E. del Valle, and F. P. Laussy, Laser Photon. Rev. **11**, 1700090 (2017).
[20] Z. A. Peng, G. Q. Yang, Q. L. Wu, and G. X. Li, Phys. Rev. A **99**, 033819 (2019).
[21] A. Gonzalez-Tudela, F. P. Laussy, C. Tejedor, M. J. Hartmann, and E. del Valle, New J. Phys. **15**, 033036 (2013).
[22] G. S. Agarwal, in *Springer Tracts in Modern Physics*, edited by G. Höhler (Springer, Berlin, 1974).

[23] H. J. Kimble, M. Dagenais, and L. Mandel, Phys. Rev. Lett. **39**, 691 (1977).

[24] N. Gisin, J. Mod. Opt. **40**, 2313 (1993).

[25] T. A. Brun and N. Gisin, J. Mod. Opt. **43**, 2289 (1996).

[26] H.-P. Breuer, B. Kappler, and F. Petruccione, Phys. Rev. A **56**, 2334 (1997).

[27] G. Bel and F. L. H. Brown, Phys. Rev. Lett. **102**, 018303 (2009).

[28] Here we consider sensors which all couple to the field radiated in the same direction, but a generalization to two-direction photon-photon correlations can be obtained by introducing sensors which couple to the field (5) emitted in different directions.

[29] C. Gardiner and P. Zoller, *The Quantum World of Ultra-Cold Atoms and Light Book I: Foundations of Quantum Optics* (Imperial College Press, London, 2014).

[30] L. Ortiz-Gutiérrez, R. C. Teixeira, A. Eloy, D. F. da Silva, R. Kaiser, R. Bachelard, and M. Fouché, New J. Phys. **21**, 093019 (2019).

[31] D. Ferreira, R. Bachelard, W. Guerin, R. Kaiser, and M. Fouché, Am. J. Phys. **88**, 831 (2020).

[32] J. Johansson, P. Nation, and F. Nori, Comput. Phys. Commun. **183**, 1760 (2012).

[33] J. Johansson, P. Nation, and F. Nori, Comput. Phys. Commun. **184**, 1234 (2013).

[34] G. Compagno, R. Passante, and F. Persico, in *Atom-Field Interactions and Dressed Atoms*, edited by R. J. R. Singer (Cambridge University Press, Cambridge, 1995).

[35] E. Jaynes and F. Cummings, Proc. IEEE **51**, 89 (1963).

[36] M. Brune, F. Schmidt-Kaler, A. Maali, J. Dreyer, E. Hagley, J. M. Raimond, and S. Haroche, Phys. Rev. Lett. **76**, 1800 (1996).

[37] A. Cipris, N. A. Moreira, T. S. do Espirito Santo, P. Weiss, C. J. Villas-Boas, R. Kaiser, W. Guerin, and R. Bachelard, Phys. Rev. Lett. **126**, 103604 (2021).

[38] H. F. Arnoldus and G. Nienhuis, J. Phys. B: At. Mol. Phys. **17**, 963 (1984).

[39] J. C. L. Carreño, E. Z. Casalengua, F. P. Laussy, and E. del Valle, Quantum Sci. Technol. **3**, 045001 (2018).

[40] L. Hanschke, L. Schweickert, J. C. L. Carreño, E. Schöll, K. D. Zeuner, T. Lettner, E. Z. Casalengua, M. Reindl, S. F. C. da Silva, R. Trotta, J. J. Finley, A. Rastelli, E. del Valle, F. P. Laussy, V. Zwiller, K. Müller, and K. D. Jöns, Phys. Rev. Lett. **125**, 170402 (2020).

[41] C. L. Phillips, A. J. Brash, D. P. S. McCutcheon, J. Iles-Smith, E. Clarke, B. Royall, M. S. Skolnick, A. M. Fox, and A. Nazir, Phys. Rev. Lett. **125**, 043603 (2020).

[42] C. Sanchez Muñoz, E. del Valle, C. Tejedor, and F. P. Laussy, Phys. Rev. A **90**, 052111 (2014).

[43] M. Peiris, B. Petrak, K. Konthasinghe, Y. Yu, Z. C. Niu, and A. Muller, Phys. Rev. B **91**, 195125 (2015).

[44] P. Grangier, G. Roger, A. Aspect, A. Heidmann, and S. Reynaud, Phys. Rev. Lett. **57**, 687 (1986).

[45] G. S. Agarwal and K. T. Kapale, J. Phys. B: At., Mol. Opt. Phys. **39**, 3437 (2006).

[46] J. Cho, Phys. Rev. Lett. **99**, 020502 (2007).

[47] D. D. Yavuz and N. A. Proite, Phys. Rev. A **76**, 041802(R) (2007).

[48] A. V. Gorshkov, L. Jiang, M. Greiner, P. Zoller, and M. D. Lukin, Phys. Rev. Lett. **100**, 093005 (2008).

[49] J. A. Miles, Z. J. Simmons, and D. D. Yavuz, Phys. Rev. X **3**, 031014 (2013).

[50] Y. Wang, S. Subhankar, P. Bienias, M. Łacki, T.-C. Tsui, M. A. Baranov, A. Gorshkov, P. Zoller, J. V. Porto, and S. L. Rolston, Phys. Rev. Lett. **120**, 083601 (2018).

[51] S. Subhankar, P. Bienias, P. Titum, T.-C. Tsui, Y. Wang, A. V. Gorshkov, S. L. Rolston, and J. V. Porto, New J. Phys. **21**, 113058 (2019).

[52] T.-C. Tsui, Y. Wang, S. Subhankar, J. V. Porto, and S. L. Rolston, Phys. Rev. A **101**, 041603(R) (2020).